

# SIDIS Multiplicity: Approval Plots

Giovanni Angelini

August 2021

## 1 Introduction

I am requesting the approval of the following plots to show in the next conferences.

**1.1 Multiplicity Definition:** The differential multiplicity for charged pions, is defined as the ratio between the differential semi-inclusive cross section and the inclusive one. After  $\phi_h$  integration, it is defined as:

$$\frac{d^4 M^{\pi^\pm}(x, Q^2, z, P_T^2)}{dx dQ^2 dz dP_T^2} = \left( \frac{d^4 \sigma^{e\pi^\pm X}}{dx dQ^2 dz dP_T^2} \right) / \left( \frac{d^2 \sigma^{eX}}{dx dQ^2} \right). \quad (1)$$

From an experimental point of view, the multiplicities are evaluated as the ratio of the hadron yields ( $N^{\pi^\pm}$ ) measured in each bin of  $(Q^2, x, z, P_T^2)$ , and the number of DIS events  $d^2 N^{DIS}$  in a given  $(Q^2, x)$  bin. Within a  $(Q^2, x)$  bin, the multiplicity is computed as follows:

$$\frac{d^2 M^{\pi^\pm}(z, P_T^2)}{dz dP_T^2} = \frac{1}{d^2 N^{DIS}} \frac{d^2 N^{\pi^\pm}(z, P_T^2)}{dz, dP_T^2} \frac{1}{a^{\pi^\pm}(z, P_T^2)}, \quad (2)$$

Therefore, it requires measuring  $e\pi X$  events, to compute acceptances and efficiencies of pions, and to compute  $eX$  events.

## 2 Data Selection

The analysis is performed on Fall 2018 in-bending data set, using the old SIDIS Monte-Carlo (MC) produced for the first publications.

The fiducial cuts already approved, used for the first publications, have been made tighter by identifying regions of CLAS12 where the detector responses are similar in Monte-Carlo simulations and in data.

For the calculation of acceptances, it is necessary to control that the detector's response in MC and data are comparable. With this in mind, I have developed tighter cuts on the PCAL coordinates, on the Drift Chamber coordinate and on the vertex. In addition, only pions up to momenta of 3 GeV/c have been considered for the analysis, since only the Time-Of-Flight detector has been used for the particle identification (PID) and study performed on the Time of flight responses in MC and data have shown discrepancies above 3GeV<sup>1</sup>.

**1. PCAL Cuts Refinements** In order to define a fiducial volume in the calorimeter, I have studied the correlation between sampling fraction and local calorimeter coordinates along the three stereo readout planes ( $lu$ ,  $lv$ ,  $lw$ ) as done for the first publications; however, this study has been performed in each sector and in different bins of momentum and angle. Since the average Sampling Fraction (SF) of the cluster is expected to be at  $SF \approx 0.25$ , if a cluster has a lower sampling function it means that the shower is not completely reconstructed, and it will be excluded from the analysis. In addition, I have required that the cut along the  $lu$ ,  $lv$ , and  $lw$  coordinates should be such to contain the whole cluster.

Figure 1 shows an example of the sampling fraction vs  $lv$ , for electrons in Sector 2 with polar angle  $12^\circ \leq \theta < 15^\circ$  in three different momentum bins.

---

<sup>1</sup>such studies are not reported here but have been presented in previous meetings

By slicing the plot in the figure, and looking at the position of the center of the cluster as well as the cluster dimension along the  $lv$  coordinate, I have defined the following fiducial cuts:  $lv < 19$  cm in data, and  $lv < 18$  cm in Monte Carlo. The cut at 19 cm on the data was the one used for the first publications under the nomenclature of "tight PCAL cut". I have then performed this study as a function of the momentum and angle and for the different sectors; I found no dependence on sector for the momentum and angle of the electron. However, in some sectors, the calorimeter has some dead areas as shown on the right column of Figure 1, where in data the strips between 97 cm and 119 cm are not working properly, therefore these strips have been removed also from the MC simulations. I have repeated these studies for the  $lw$  coordinates. The same minimum cut developed for the  $lv$  coordinate applies well also to the  $lw$  coordinate (i.e.,  $lw < 19$  cm) and no sector momentum or angle dependence has been found. Also, in this case, a maximum cut should be applied to avoid the region where the calorimeter has dead strips.

No cut has been applied along the  $u$  strips of the calorimeter, since the  $lu$  direction is determined by  $lv$ , and  $lw$ .

In summary, the EC fiducial cuts we have applied in my analysis are:

- In all Sectors:  $lv, lw > 18$  cm in MC ;  $lv, lw > 19$  cm in Data.
- Sector 1 :  $69 < lw < 97$  cm in MC;  $70 < lw < 98$  cm in Data.
- Sector 2 :  $96 < lv < 118$  cm in MC ;  $97 < lv < 110$  cm in Data.

**2. Drift Chamber Refinement Cuts** In order to refine the drift chamber cuts, I have studied the number of events with assigned PID with respect to all the charged tracks not associated with electrons. Specifically, after applying standard fiducial cuts on the Drift Chambers, I have computed

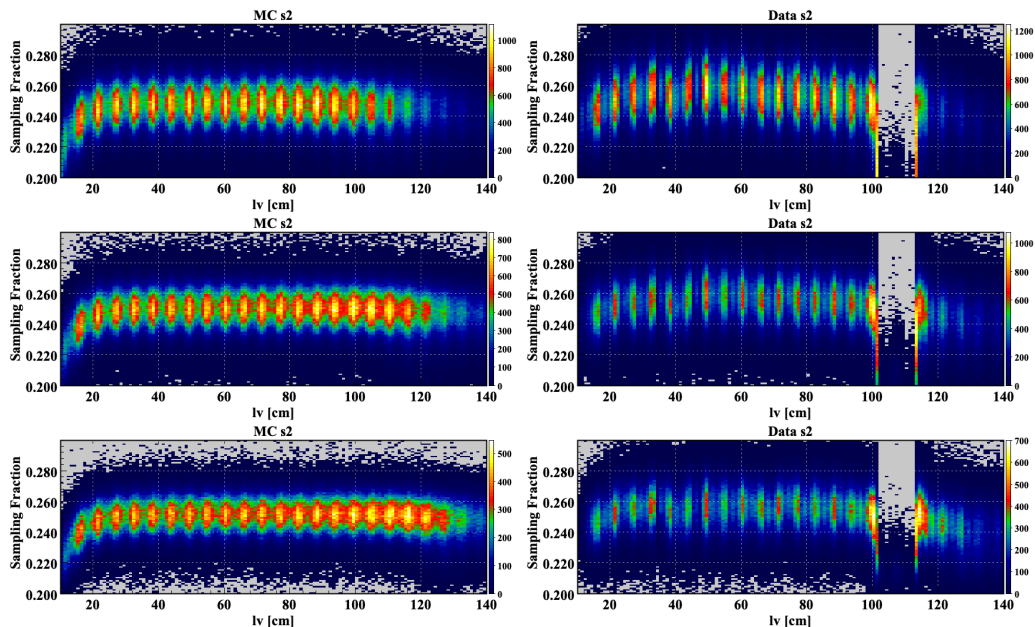


Figure 1: Left column: Electron Sampling Fraction vs  $lv$  coordinate of the PCAL (Sector 2) in Monte-Carlo simulations. Right column: Electron Sampling Fraction vs  $lv$  coordinate of the PCAL (Sector 2) in Data. Each row represents a different momentum bin. In the first row, the electrons have  $3 \text{ GeV} < p < 4 \text{ GeV}$  and  $15^\circ \leq \theta \leq 18^\circ$ . In the second row, electrons have  $4 \text{ GeV} < p < 5 \text{ GeV}$  and  $15^\circ \leq \theta \leq 18^\circ$ . In the third row, electrons have  $5 \text{ GeV} < p < 7 \text{ GeV}$  and  $15^\circ \leq \theta \leq 18^\circ$ . In the data, the strip between 97 and 119 are inactive in the data.

the number of identified charged hadrons (i.e., pions and kaons identified by the Event Builder) with respect to the total number of charged tracks (but excluding the tracks associated to electrons). This number represents how many charged tracks have been successfully identified as particle from the event builder. By comparing this ratio in MC and in data, it is possible to identify region where the Event Builder acts differently, and therefore the acceptances computed from MC cannot be applied to the data. As an example,

Fig. 2 shows such histograms for MC and data in the case of positive tracks as function of the x-y components of the DC Layer 1 <sup>2</sup>. On the left of the picture it is shown the number of tracks with associated PID in data, in the central picture is shown the number of tracks with associated PID in MC, and on the plot on the right is shown the ratio of the other two histograms. It is clear that while the MC shows a more uniform distribution across the drift chambers (see the extended red region), in the data the tracks that hit the farthest part of the Drift Chamber show a decrease in PID efficiency. The region where the discrepancy of MC and data is more than 10% have been removed from the analysis. Studies have been performed by slicing the histograms in the previous Figure and perform careful comparisons, but are not shown in this short document. As results of these studies, we have applied two circular cuts on the DC layer 1 (at radius 60 cm and 120 cm). The study has been performed also on the other layers of the DC but after applying the cut on the first layer all the other get cleared out. The study has been repeated for negative tracks as well.

**3. Vertex Cut** The vertex cut has been defined for electron and pions, by performing a fit of the vertex z-component as function of sector, momentum and angle of the particle under study. The fit has been performed using a step functions (representing the target cell) convoluted with a Gaussian (representing the vertex reconstruction resolution). An example of the electron vertex comparison for data and MC is shown in Fig. 3 where for sector 4 and fixed polar angle bin, the z-component of the vertex is shown as function of the electron momentum. In the Figure, M represents the mean position of the Gaussian, W the width of the step function, and S the standard deviation

---

<sup>2</sup>meaning that I have projected the tracks to the DC layer 1 and then computed the ratio of how many were reconstructed by EB

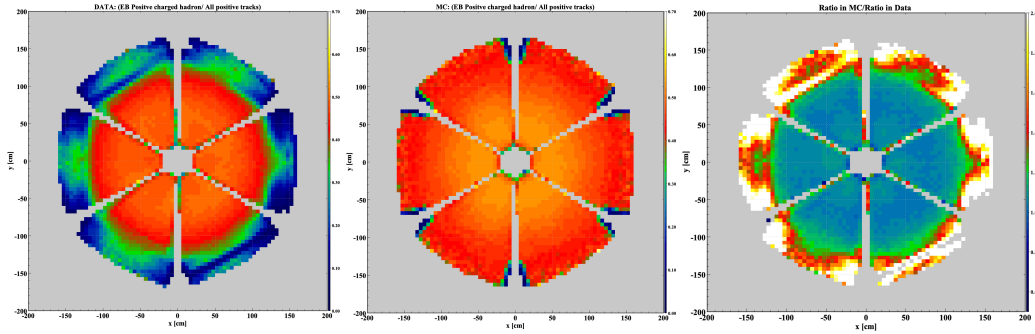


Figure 2: The ratio of positive charged hadron tracks identified by the event builder with respect to the overall negative tracks. The tracks identified as electrons have been removed from the sample. The result for data is shown in panel (a), while for the simulation in panel (b). In panel (c) the ratio of results for MC and data is shown. Clearly, at very low polar angle and high polar angle, there are significant discrepancies between the quantity of reconstructed tracks.

of the Gaussian.

**4. Other differences with respect to common RG-A cuts** In the common cuts used for the first publications a Chi2PID cut was used, such cut was as function of momentum. In this case, since we stop at 3 GeV of momentum, that cut has been removed.

### 3 Results

The analysis has been performed by binning  $Q^2$ ,  $x$ ,  $z$ , and  $P_T^2$ . The  $(Q^2, x)$  plane has been divided in 14 regions as shown in Fig. 4, where the kinematics of semi inclusive electrons are shown together with the bin number and the kinematic limits of each bin. The  $z$  variable has been binned at an interval

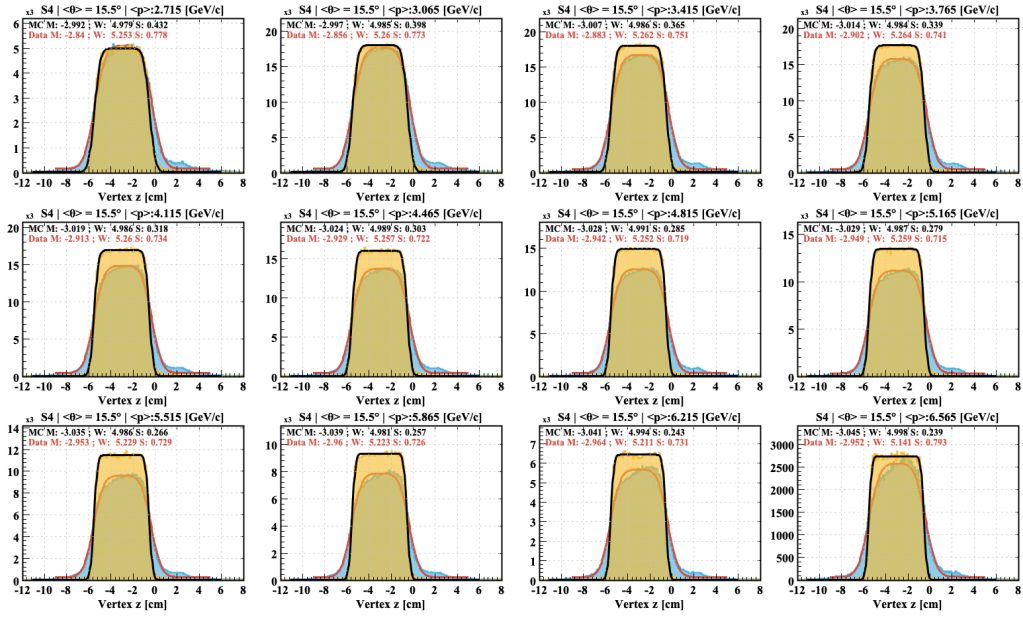


Figure 3: Electron vertex  $z$  component in data (blue histogram) and MC (yellow histogram) for electron of average polar angle of  $15.5^\circ$ . Each plot represents a different average momentum. The red line represents a fit of a Step function convoluted with a Gaussian and fitted on the data, while the black line is a fit performed on the MC.

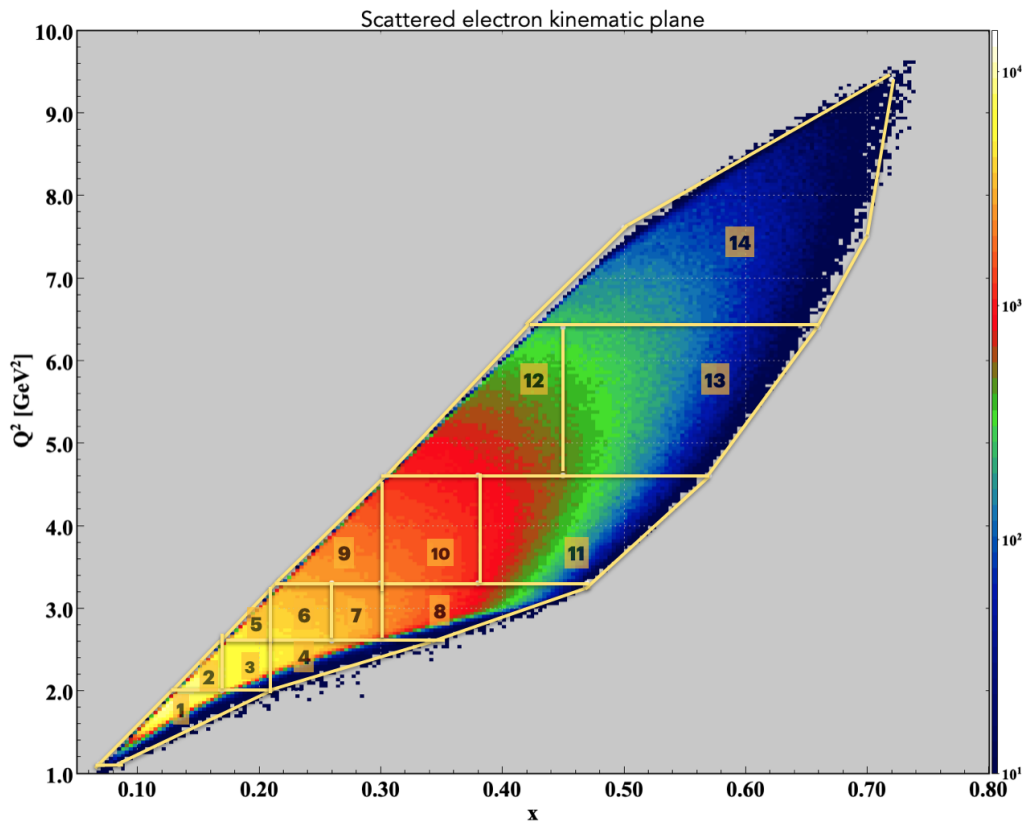


Figure 4: The  $Q^2$ ,  $x$  phase space after fiducial cuts for semi-inclusive electrons. The figure shows the 14 bins used for the analysis.

of 0.05, while  $P_T^2$  in intervals of  $0.03 \text{ GeV}^2$ . The decision of this binning size has been driven by the requirements of having enough bins to study  $z$  and  $P_T^2$  dependencies without compromising the statistical uncertainty and the bin purity. The bin purity is defined as the amount of the events generated and reconstructed in a bin, with respect to all the events reconstructed in such a bin. Extensive studies have been performed on the influence of the purity from the bin size, but are not presented in this document. The  $\pi^+$  multiplicity obtained for bin 1, 5 and 12 is shown respectively in Fig. 5, Fig. 6, and Fig. 7. These are the Figure I am asking approval for release.

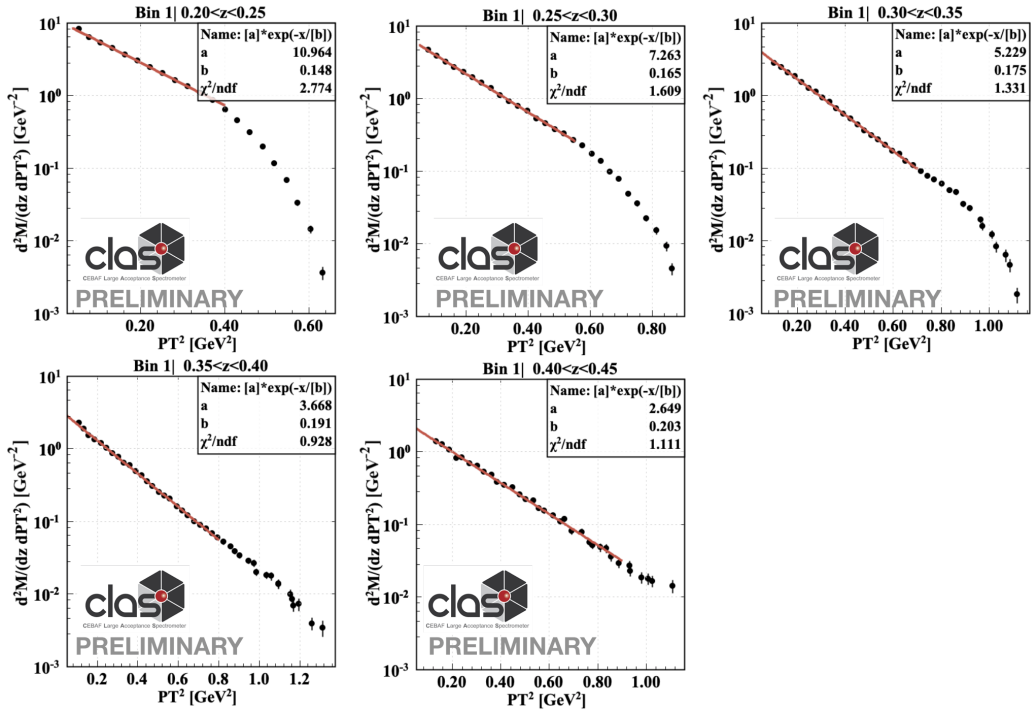


Figure 5: The  $\pi^+$  multiplicity as function of transverse momentum for different  $z$  bins in the first bin of the  $(x, Q^2)$  plane :  $\langle Q^2 \rangle = 1.8 \text{ GeV}^2$ ,  $\langle x \rangle = 0.13$ .

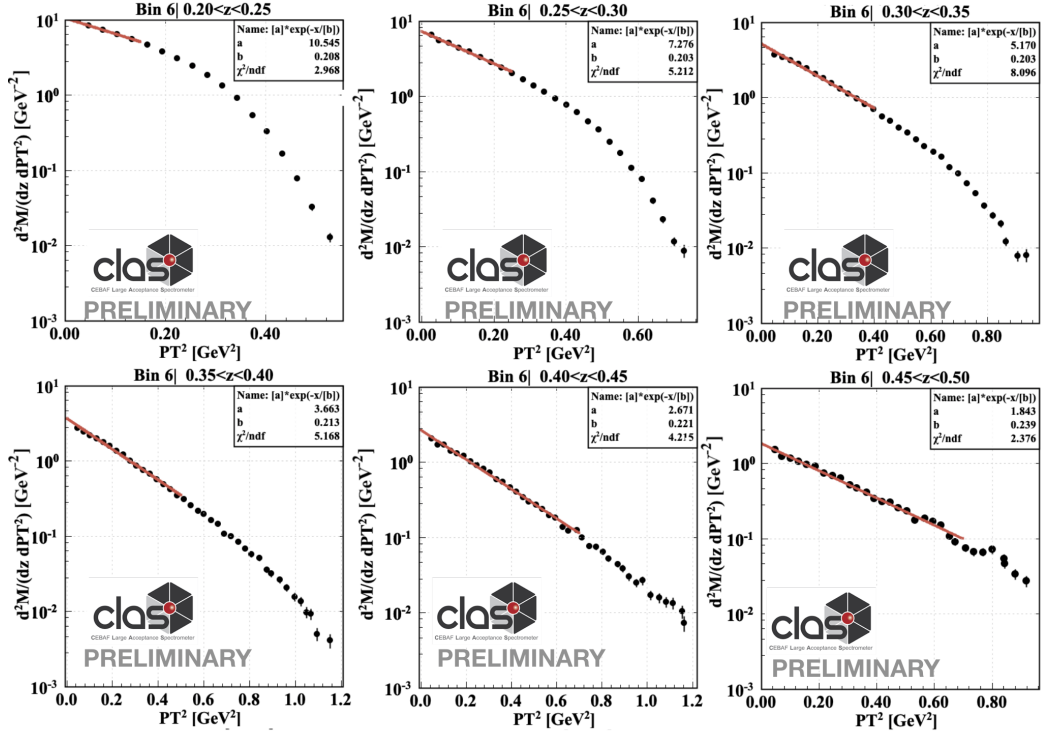


Figure 6: The  $\pi^+$  multiplicity as function of transverse momentum for different  $z$  bins in the sixth bin of the  $(x, Q^2)$  plane:  $\langle Q^2 \rangle = 2.9 \text{ GeV}^2$ ,  $\langle x \rangle = 0.23$ .

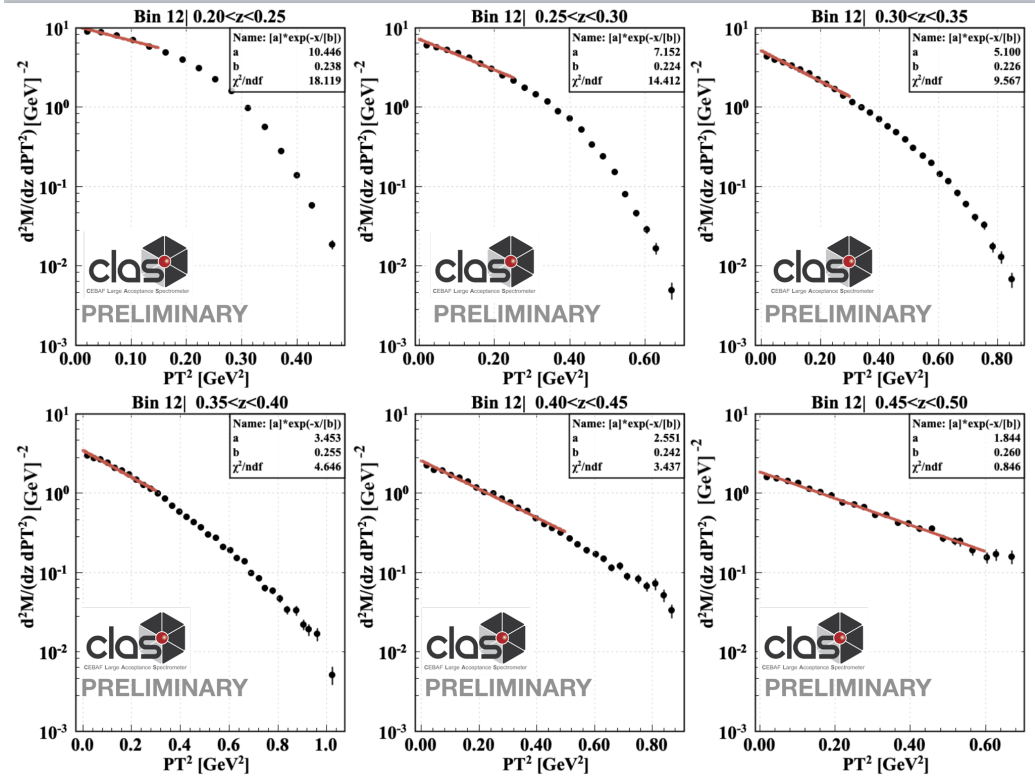


Figure 7: The  $\pi^+$  multiplicity as function of transverse momentum for different  $z$  bins in the twelve bin of the  $(x, Q^2)$  plane:  $\langle Q^2 \rangle = 5.2 \text{ GeV}^2$ ,  $\langle x \rangle = 0.40$ .